applied sciences

MDPI

Article

Prediction of Seismic Bearing Capacity Considering Nonlinearity and Dilatancy by Sequential Quadratic Programming

Hong Liao and De Zhou *

School of Civil Engineering, Central South University, Changsha 410075, China
* Correspondence: 210026@csu.edu.cn

Abstract: Most of the published literature regarding bearing capacity are often focused on linear and associative soils. Concerning the intrinsic strength nonlinearity in dilatancy soils, this study investigates the problem of the seismic bearing capacity in the framework of the kinematic theorem of limit analysis. The conventional linear Mohr–Coulomb criterion is substituted with a nonlinear power law criterion to depict the nonlinearity of the soil strength. The non-associative feature of soil materials is considered by defining a nonlinear dilatancy coefficient. A generalized tangential technique is accordingly introduced to linearize the strength envelope for making the nonlinear criterion tractable in the analysis. A non-symmetrical translational failure mechanism that is comprised of several rigid wedges is used to characterize the failure of the foundation at the limit state. Moreover, the seismic action is considered by the classic pseudo-static method. Based upon the energy equilibrium theory of the upper-bound limit analysis, new analytical solutions are derived from the work-balanced equation with nonlinearity and dilatancy. This rigorous upper-bound solution is formulated as a multivariate optimization problem and is readily addressed by sequential quadratic programming (SQP). To verify the reliability of the new expressions, the present results are compared with already posted solutions and the original pseudo-dynamic solutions. The comparative results show a good agreement with previous works, and the correctness and rationality of the new analytical solutions are validated. The detailed parametric study reveals that, in the non-associative flow soils, the ultimate bearing capacity is significantly decreased with a reduction in the dilatancy coefficient. Particularly in the linear condition, namely m = 1, the larger the internal friction angle is, the more obvious the influence of the non-associative feature on the bearing capacity is.

Keywords: seismic bearing capacity; shallow foundations; multi-block mechanism; kinematic theorem

Citation: Liao, H.; Zhou, D. Prediction of Seismic Bearing Capacity Considering Nonlinearity and Dilatancy by Sequential Quadratic Programming. *Appl. Sci.* **2023**, *13*, 3215. https://doi.org/10.3390/app13053215

Academic Editor: Cheng-Yu Ku

Received: 12 February 2023
Revised: 25 February 2023
Accepted: 28 February 2023
Published: 2 March 2023

1. Introduction

The foundation is the mainstay that directly bears the load transferred from the superstructure. It plays an important role in maintaining the safety and stability of the whole structure since the outcome and casualties are immeasurable once the failure of the foundations suddenly occurs, especially suffering from natural hazards such as earthquake striking. Therefore, the influence of earthquakes on the seismic safety of shallow strip footings draws much attention. Earlier, numerous efforts on the seismic bearing capacity have been made by several researchers with various methods [1–8].

Concerning the description of seismic acceleration, several proposals were put forward, such as the conventional pseudo-static method, pseudo-dynamic method and its modification, or directly inputting the seismic signal in a numerical simulation [9–17]. Recently, Keshavarz and Nemati [18] studied the seismic ultimate bearing capacity of strip footing resting on reinforced soils using a pseudo-static method by the stress characteristics method. The same procedure was applied to foundations resting on rock following the Hoek–Brown criterion by Keshavarz et al. [19]. Additionally, Casablanca et al. [20]

revisited the problem of static and seismic bearing capacity factors of foundations placed on slopes, where the influence of the earthquake wave-induced loads in soils and inertia forces resulting from the structural dynamic response are analyzed separately. As for the limit equilibrium method, Ghosh and Debnath [21] conducted a seismic analysis of the soil–foundation system in M-C materials. A bearing capacity coefficient related to weight, surcharge, and cohesion was formulated. Izadi et al. [22] considered the effect of undrained shear strength varying with depth on the bearing capacity of foundations and derived the seismic bearing capacity of shallow strip footing on heterogeneous marine deposits. Nouzari et al. [23] studied the bearing capacity of foundations overlying the unsaturated soil deposits, which made the field research more complete. Note that the seismic analysis in the aforementioned contributions was considered by the pseudo-static method, which directly reflects that the application of the pseudo-static method is still predominant.

In addition, based on the limit analysis method, Qin and Chian [24] established a discretization-based technique to address the seismic stability problem in a non-uniform soil slope by a pseudo-dynamic approach; then, the same discretization technique was applied to a similar circumstance for estimating the bearing capacity of the slope which suffers from Rayleigh waves (a kind surface wave forming in the process of the body wave propagates to the surface). Such a seismic analysis considered the dynamic properties of earthquake waves and provided a comprehensive understanding of how the dynamic parameters influence the ultimate bearing capacity of the slopes. However, the accuracy of the solution only improved by 5%, and this improvement seems inconspicuous. Moreover, the theorem of the aforementioned pseudo-dynamic analyses is still defective, such as the violation of the zero-stress boundary condition, being unable to consider the damping of geomaterials, and the assumption of a constant amplitude amplification factor not being thoroughly addressed. Moreover, the structure design in practice tends to be conservative so that one can provide a safer result. Thus, the classic pseudo-static method is adopted in this paper instead of the pseudo-dynamic method.

Apart from the external adverse factors [25–30], the inherent nonlinearity of soil strength and the non-associative characteristics of plastic flow is also necessary to be paid attention to [30–32]. In reality, amounts of geotechnical tests and experiments have shown that the strength envelope of soils is often nonlinear in various stress states due to the sedimentary condition and stress history, and the plastic flow of dilatancy soils is not always associative. Therefore, several nonlinear failure criteria, such as the power law (PL) criterion for soils and the Hoek–Brown criterion and its modified forms for rock masses, are proposed to account for this characteristic in the stress–strain space. To make the nonlinear criteria tractable in theoretical analysis, Zhang and Chen [33] proposed a generalized tangential technique to calculate the equivalent Mohr–Coulomb (M-C) strength parameters and evaluate the slope stability. In practice, the plastic flow of geomaterials at a limit failure state usually shows non-associated characteristics. In view of this, Drescher and Detournay [34] defined a nonlinear dilatancy coefficient ζ to consider the non-associative feature of materials which keeps the associative flow rule unchanged. Then, those methods were extended to assess stability problems under nonlinear failure criteria with more complicated conditions involving slopes with cracks, water pressure, and tunnel excavation, etc. [35–42].

Prior to the analysis, the failure mechanism is necessary to be determined first. According to the situation, whether the seismic loading is considered or not, the failure mechanism of shallow foundations consists of two types: one is the symmetrical mechanism that applies to seismic conditions, while the other is non-symmetrical that is capable of handling the earthquake action. For addressing the bearing capacity problem under seismic conditions, Soubra [43] proposed two multi-block translational mechanisms. One of the multi-block mechanisms is non-symmetrical and is used for a seismic situation; it consists of a certain number of rigid blocks that can slide with each other in the limit state, which makes the failure of the foundation easier to achieve and can derive a fine upper-bound solution. Therefore, this study focuses on the influence of the strength non-

linearity and dilatancy of geomaterials on the ultimate bearing capacity of foundations using the non-symmetrical multi-block mechanism and pseudo-static method. Then, a closed-form analytical expression of the bearing capacity of strip footings is derived from the equilibrium between the internal energy dissipation and the external work rate. This solution is determined by 2n + 1 dependent variables, which are difficult to be accurately solved; therefore, an optimization toolbox embedded in MATLAB software is adopted to search for the least upper-bound solution. Moreover, a direct optimization procedure is used to find the best bearing capacity instead of the superposition method that calculates the bearing capacity factors, respectively. The detailed implementation of this work is provided in the following sections.

2. Methodology

2.1. Kinematic Theorem of Limit Analysis

It is shown that, after long-term development and improvement, the limit analysis theorem has been widely accepted by researchers and designers due to its rigorous theory and robustness. Chen [44] initially summarized the existing contributions of limit analysis and provided a systematic elaboration of the theoretical background, formula derivation, and practical application. It is known that the principal part of limit analysis is made up of the kinematic theorem which addresses the geotechnical engineering problem from the perspective of kinematics and the stress equilibrium theorem which solves the equilibrium problem in the context of stress analysis. Because of the intrinsic theory feature of the limit analysis, the kinematic method is capable of addressing the problems analytically and is usually preferred by scholars while the lower bound method focuses on establishing a statically permissible stress field which is complicated to construct analytically and is usually solved by the finite element method.

In this section, only the kinematic approach of the limit analysis is taken into consideration. Some basic assumptions are made as follows to accommodate for the applicability of the kinematic limit analysis. The soil materials in the limit state present an ideal elastic-plastic deformation and the plastic flow respects the normal flow rule. Assuming the principal rate of the plastic strain and principal stress is coaxial, the following relationship between stress and the rate of strain is derived from the associated flow rule and the normality of the yield function:

$$\dot{\varepsilon}_{ij} = \dot{\lambda}\frac{\partial f\left(\sigma'_{ij}\right)}{\partial \sigma'_{ij}},\ \dot{\lambda} \geq 0 \tag{1}$$

where $\dot{\varepsilon}_{ij}$ is the rate of the plastic strain, σ'_{ij} is the effective stress, $f\left(\sigma'_{ij}\right) = 0$ is the yield function, and $\dot{\lambda}$ is a non-negative coefficient. The upper-bound theorem typically takes the following form:

$$\int_V \sigma_{ij}\dot{\varepsilon}_{ij}\mathrm{d}V \geq \int_S T_i v_i \mathrm{d}S + \int_V F_i v_i \mathrm{d}V \tag{2}$$

where T_i and F_i denote the external loads that apply to the surface S and volume V, respectively, v_i represents a kinematically admissible velocity field, σ_{ij} is effective stress, and $\dot{\varepsilon}_{ij}$ is the plastic strain rate along the plastic shear band. Solving this equation, a closed-form limit load that is no less than the true limit load can be derived.

2.2. Nonlinear Failure Criterion of Dilatancy Soils

The nonlinearity of the soil strength, as a common existence in the natural environment, has been found by numerous laboratory tests and in situ tests. After constantly fitting from trial and error, the generalized form of the nonlinear failure criterion can be typically presented as a P-L expression for the soil materials in $\sigma_n - \tau$ stress space:

$$\tau = c_0\left(1 + \frac{\sigma_n}{\sigma_t}\right)^{\frac{1}{m}} \tag{3}$$

where σ_n and τ denote the stress state in the slip surface at failure, σ_t represents the uniaxial tensile strength which can be derived from the experiment, the physical meaning of c_0 is the initial cohesion, and m is a dimensionless coefficient that describes the degree of the nonlinearity of the strength envelope; when $m = 1$, the above nonlinear criterion becomes the linear M-C criterion. There are no proper measures to directly apply the nonlinear criterion to the analysis so far. Several linearized methods can be found in the literature, such as the equivalent M-C parameters method, tangential technique, and piecewise linear method, among which the tangential technique is widely applied in the limit analysis because of its advantage of a clear concept and easy implementation. Therefore, the tangential technique developed by Zhang and Chen [33] and Yang and Yin [45] is adopted in this work. Introducing a tangential line to linearize the nonlinear strength criterion makes the nonlinear envelope tractable. As illustrated in Figure 1, for a random straight line that is tangent to the nonlinear envelope at point P, the tangential equation reads:

$$\tau_t = c_t + \sigma_n \tan \varphi_t \tag{4}$$

where c_t and φ_t represent the equivalent cohesion and internal friction angle, and based on the geometry relationship, the corresponding shear strength parameters have the following relationship with the parameters of the P-L failure criterion.

$$c_t = \frac{m-1}{m} c_0 \left(\frac{m\sigma_t \tan \varphi_t}{c_0} \right)^{1/(1-m)} + \sigma_t \tan \varphi_t \tag{5}$$

This linearization operation makes the nonlinear strength envelope represented by the amounts of tangents, and each solution obtained by a tangent is proven to be a rigorous upper-bound solution, from which one can obtain the least upper-bound solution.

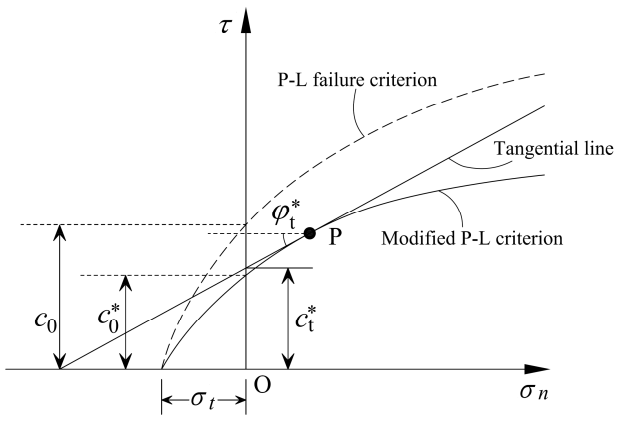

Figure 1. The modified power law strength envelope and corresponding tangential line.

2.3. Non-Associative Flow Rule

In the literature, the major geotechnical problems were analyzed in the geomaterials governed by the associative flow rule. However, it is recognized that the plastic flow in the limit state behaves as a non-associative feature for real soils [34,46]. At present, there are two main research ideas to consider the non-associative characteristics of materials in the limit analysis: (1) use the non-associative flow rule directly for the calculation without changing the yield criterion, and (2) keep the associative flow rule unchanged and modify the parameters in the yield criterion or introduce a variable to represent the non-associative characteristics. In practice, the calculation process of the former is usually complex, and the trickier point is that the non-associative flow method does not satisfy the basic assumptions of the limit analysis principle, which makes it difficult to continue the analysis. The latter has a clear idea and method and is more suitable for combining with the upper-bound principle. Therefore, following the second research idea, a nonlinear dilatancy coefficient

ζ proposed by Drescher and Detournay [34] is introduced in this work to improve the strength criterion, and the shear strength parameters can be modified by the following expression:

$$\begin{cases} c^* = \zeta c \\ \tan\varphi^* = \zeta \tan\varphi \end{cases} \tag{6}$$

where c^* and φ^* represent the shear strength parameters of the materials that satisfy the non-associative flow rule; ζ denotes the dilatancy coefficient and is defined as:

$$\zeta = \frac{\cos\varphi\cos\psi}{1-\sin\varphi\sin\psi} \tag{7}$$

where ψ is the dilatancy angle during the plastic shearing failure, which ranges from 0 to φ. According to Equation (7), the coefficient ζ reaches the maximum value, namely 1, when $\psi = \varphi$, which is also the case that the plastic flow rule changes from non-associative to associative. Such an introduction of the dilatancy coefficient makes the M-C criterion applicable to the non-associative material. Accordingly, the P-L criterion is also revised to portray the nonlinearity and non-associative flow characteristics of the materials.

$$\tau = \zeta c_0 \left(1 + \frac{\sigma_n}{\sigma_t}\right)^{\frac{1}{m}} \tag{8}$$

Applying the derivation operation to Equation (8) about σ_n, the tangent slope yields:

$$\tan\varphi_t^* = \frac{\mathrm{d}\tau}{\mathrm{d}\sigma_n} = \frac{\zeta c_0}{m\sigma_t}\left(\frac{\sigma_n}{\sigma_t} + 1\right)^{(1-m)/m} \tag{9}$$

By rearranging Equations (4), (8), and (9) and eliminating the stress components from the equations, an expression that only contains the shear strength parameters c_t^* and φ_t^* is expressed as:

$$c_t^* = \frac{m-1}{m}\zeta c_0 \left(\frac{m\sigma_t \tan\varphi_t^*}{\zeta c_0}\right)^{1/(1-m)} + \sigma_t \tan\varphi_t^* \tag{10}$$

3. Pseudo-Static Analysis of Ultimate Bearing Capacity

The implementation of the upper-bound limit analysis entails the first establishment of a kinematically admissible velocity field, thus, a shallow strip footing that is placed on the homogeneous geomaterial governed by the P-L criterion is depicted in Figure 2. The buried depth from the footing level to the ground surface is D and the width is B. The bottom of the foundation is presumed to be rough. The lateral soil pressure is equivalent to uniformly distributed loads denoted as $p = \gamma D$. In the presence of an earthquake, a non-symmetrical failure is prone to happen due to the existence of a horizontal seismic load, whereby a non-symmetrical multi-block translational mechanism is necessarily established. The inertia forces acting on the lateral covering layer are considered as two uniformly distributed loads that are perpendicular to the surface and parallel to the surface, respectively. It is common sense to the researchers that decreasing the soil strength and/or raising the failure loads are two primary forms by which the earthquake action influences the soil–foundation system. Herein, only the latter is taken into consideration.

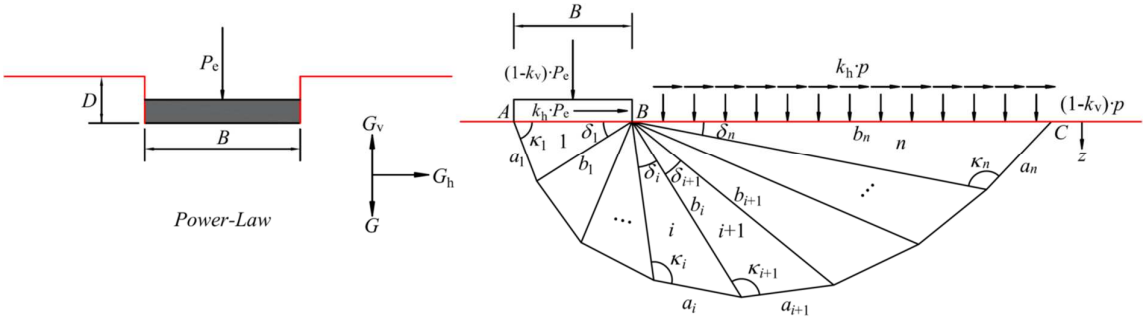

Figure 2. Sketch map of shallow foundation failure mechanism under the seismic condition.

Figure 2 shows a simple sketch map of a shallow foundation in a broken state. The whole failure region is decomposed into a multi-block collapse mechanism that is comprised of n rigid wedges with point B as the same vertex. The first rigid block lying at the bottom of the strip footing translates in the meantime with footing without relative sliding, and the last block terminates at the footing level BC. The relative sliding between the successive blocks along the contacted face is permitted. The geometry shape of each block is determined by total $2n$ independent angular parameters δ_i and κ_i.

Then, the kinematic analysis of the rigid blocks is developed herein to formulate the energy equilibrium equation. The associative flow rule requires that materials in the plastic flow state should possess the property that the rate of plastic strain is perpendicular to the yield surface. This requests a normal detaching velocity along the contacted face, which results in an inclined angle φ_t^* between the relative velocity and slip surface. In this view, given the translational velocity of block 1 denoted as v_1, combining the aforementioned requirements, one can readily derive the relative velocity $v_{1,2}$ from the velocity vector triangle, as sketched in the left-hand of Figure 3. For simplicity, the generic recurrence relationships between v_i and $v_{i,i+1}$ of the ith block are presented as:

$$v_{i+1} = \frac{\sin(\delta_i + \kappa_i - 2\varphi_t^*)}{\sin(\kappa_{i+1} - 2\varphi_t^*)} \cdot v_i \tag{11}$$

$$v_{i,i+1} = \frac{\sin(\delta_i + \kappa_i - \kappa_{i+1})}{\sin(\kappa_{i+1} - 2\varphi_t^*)} \cdot v_i \tag{12}$$

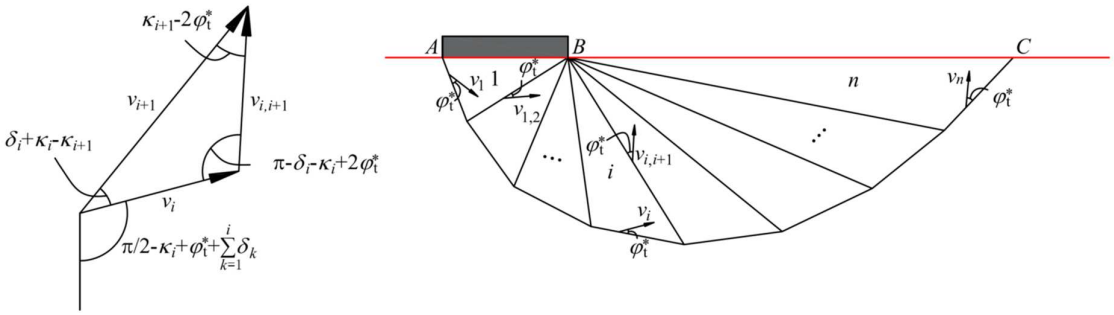

Figure 3. Velocity vector diagram of failure blocks.

In analogy, the lengths of the slip surface a_i and b_i of the ith wedge can be readily derived:

$$a_i = \frac{\sin\delta_i}{\sin(\delta_i + \kappa_i)} b_{i-1} \tag{13}$$

$$b_i = \frac{\sin\kappa_i}{\sin(\delta_i + \kappa_i)} b_{i-1} \tag{14}$$

The initial values of a_1 and b_1 in the first block attribute to width B are depicted as:

$$a_1 = \frac{\sin\delta_1}{\sin(\delta_1+\kappa_1)}B \tag{15}$$

$$b_1 = \frac{\sin\kappa_1}{\sin(\delta_1+\kappa_1)}B \tag{16}$$

3.1. Rate of External Work and Internal Energy Dissipation

This subsection concentrates on the calculation of the external work rate. The external loads included in the soil–foundation system are comprised of the gravity of soil, equivalent surcharge load, loads from the superstructure, and inertia force. First, because the soil weight and inertia force are both a uniformly distributed body force that depends on the soil mass, for convenience, their work rate can be calculated together by the following expression:

$$W_\gamma = \frac{1}{2}\gamma\sum_{i=1}^{n} b_{i-1}b_i \sin\delta_i v_i \cos\theta_i \tag{17}$$

$$W_\mathrm{e} = \frac{1}{2}\gamma\sum_{i=1}^{n} b_{i-1}b_i \sin\delta_i v_i (k_\mathrm{h}\sin\theta_i - k_\mathrm{v}\cos\theta_i) \tag{18}$$

where γ denotes the unit weight of foundation soil, and θ_i denotes the inclined angle of v_i in a vertical direction, as presented in the left hand of Figure 3, and reads:

$$\theta_i = \frac{\pi}{2} - \kappa_i + \varphi_t^* + \sum_{k=1}^{i}\delta_k \tag{19}$$

Then, the work rate produced by the lateral soil pressure p is obtained by the product velocity vector and force vectors as follows:

$$W_p = pb_n v_n \sin\theta_n k_\mathrm{h} + pb_n v_n \cos\theta_n (1-k_\mathrm{v}) \tag{20}$$

Similarly, the work rate contributed by the load of the superstructure P_e is depicted by:

$$W_{P_\mathrm{e}} = P_\mathrm{e} v_1 [(1-k_\mathrm{v})\sin(\kappa_1-\varphi_t^*) + k_\mathrm{h}\cos(\kappa_1-\varphi_t^*)] \tag{21}$$

Lastly, the gross external work rates are captured by the accumulation of the components of Equations (17), (18), (20), and (21).

$$W_\mathrm{ext} = W_\gamma + W_\mathrm{e} + W_p + W_{P_\mathrm{e}} \tag{22}$$

Apart from the work rate achieved by an external force, the summation of the internal energy consumed in the thin shear band a_i and b_i yields:

$$D_\mathrm{int} = c_\mathrm{t}\cos\varphi_t^* \left(\sum_{i=1}^{n} a_i v_i + \sum_{i=1}^{n-1} b_i v_{i,i+1}\right) \tag{23}$$

3.2. Seismic Ultimate Bearing Capacity

Based upon the equilibrium between Equations (22) and (23), an analytical upper bound solution of the ultimate bearing capacity of strip footings in the presence of earthquake conditions is eventually derived in the following form:

$$P_\mathrm{e} = \left(D_\mathrm{int} - W_\mathrm{e} - W_\gamma - W_p\right) / [v_1 k_\mathrm{h}\cos(\kappa_1-\varphi_t^*) + v_1(1-k_\mathrm{v})\sin(\kappa_1-\varphi_t^*)] \tag{24}$$

For comprehensively understanding the contributions of different parameters, the normalized ultimate bearing capacity is furtherly decomposed into the following three components:

$$p_\mathrm{ce} = \frac{P_\mathrm{e}}{B} = \frac{1}{2}\gamma B \cdot N_{\gamma\mathrm{e}} + p \cdot N_{p\mathrm{e}} + c_t^* \cdot N_{c_t^*\mathrm{e}} \tag{25}$$

where $N_{\gamma e}$, N_{pe}, and $N_{c_t^* e}$ are dimensionless functions and are known as the bearing capacity factors which separately depict the significance of the soil gravity, equivalent surcharge, and cohesion on the seismic bearing capacity. The above dimensionless functions are presented in terms of the as of yet unspecified angles $2n + 1$ δ_i, κ_i, and φ_t^*

$$N_{\gamma e} = -\frac{k_h g_1 + (1 - k_v) g_2}{\cos(\kappa_1 - \varphi_t^*) k_h + (1 - k_v) \sin(\kappa_1 - \varphi_t^*)} \tag{26}$$

$$N_{pe} = -\frac{k_h g_3 + (1 - k_v) g_4}{\cos(\kappa_1 - \varphi_t^*) k_h + (1 - k_v) \sin(\kappa_1 - \varphi_t^*)} \tag{27}$$

$$N_{c_t^* e} = \frac{g_5}{\cos(\kappa_1 - \varphi_t^*) k_h + (1 - k_v) \sin(\kappa_1 - \varphi_t^*)} \tag{28}$$

The above dimensionless expressions g_i $(i = 1, 2, \ldots, 5)$ have a specific form that is referred to in Appendix A.

Note that from Equation (25), clearly the ultimate bearing capacity is determined by the $2n$ independent angular variable δ_i, κ_i and one equivalent internal frictional angle φ_t^*. Any set of these parameters will provide a certain upper-bound solution; the least one of them needs to be found by the SQP algorithm.

Since the advent of MATLAB numerical software in 1984, it has gradually developed into one of the most popular scientific and technological application software due to its simple syntax rules, powerful drawing and operation capabilities, and excellent openness. Therefore, the optimization solution in this work will be realized by using the fmincon function in the built-in toolbox of MATLAB. One can call the SQP algorithm in the fmincon function. The following is a brief introduction to the use of the fmincon function. The mathematical model of the fmincon function is:

$$\text{s.t.} \begin{cases} \min f(\boldsymbol{x}) \\ C(\boldsymbol{x}) \le 0 \\ Ceq(\boldsymbol{x}) = 0 \\ \boldsymbol{A} \cdot \boldsymbol{x} \le \boldsymbol{b} \\ \boldsymbol{Aeq} \cdot \boldsymbol{x} = \boldsymbol{beq} \\ \boldsymbol{lb} \le \boldsymbol{x} \le \boldsymbol{ub} \end{cases} \tag{29}$$

The calling format of the fmincon function in Matlab is:

$$\boldsymbol{x} = \text{fmincon}(fun, \boldsymbol{x_0}, \boldsymbol{A}, \boldsymbol{b}, \boldsymbol{Aeq}, \boldsymbol{beq}, \boldsymbol{lb}, \boldsymbol{ub}, nonlcon, options) \tag{30}$$

where *fun* is the objective function which is defined by the actual problem; $\boldsymbol{x_0}$ is the initial value of the variables; and $\boldsymbol{A}$, $\boldsymbol{b}$ $\boldsymbol{Aeq}$, $\boldsymbol{beq}$, $\boldsymbol{lb}$, and $\boldsymbol{ub}$ are the matrices that need to meet the constraint in Equation (29). Therefore, the optimization problem in this work is formulated as:

$$\begin{aligned} &\min \ p_{ce} = f(\delta_i, \kappa_i, \varphi_t^*) \\ &\text{s.t.} \begin{cases} \sum_{i=1}^{n} \delta_i = \pi, \ i = 1, 2, \ldots n \\ \delta_i + \kappa_i \ge \kappa_{i+1} \end{cases} \end{aligned} \tag{31}$$

In most previous analyses, the bearing capacity of the foundations is obtained by separately calculating Equations (26)–(28) and accumulating them. Such a superposition method tends to provide a safe estimation compared to the direct numerical optimization method; hence, the direct numerical optimization of Equation (31) is employed in this work.

4. Numerical Results and Discussions

4.1. Comparisons

The closed-form analytical solution of Equation (31) is formulated as a multivariate optimization problem where the number of optimized variables is $2n + 1$. An increase in the number of blocks indeed results in a better accuracy of the solution; however, this is directly accompanied by the burden of the computation time, thus a compromise between

the efficiency and accuracy should be accomplished. Table 1 calculates the values of seismic bearing capacity factors versus the number of blocks without considering the seismic loading. It is obvious that the ultimate bearing capacity of the foundation decreases with the number of blocks gradually increasing, and the corresponding bearing capacity factors show the same tendency as the bearing capacity. Notably, the reduction effect is significant with n varying from 2 to 5 and then slowly disappearing with a reduction of no more than 0.06% when n = 14, which indicates at this time that a further increase in the number of blocks leads to a neglectable positive effect on the upper bound solution and results in great time consumption. Therefore, a mechanism of 14 blocks is adopted in the later development.

Table 1. Values of bearing capacity factors versus the number of blocks.

n	$N_{\gamma e}$	N_{pe}	N_{ce}	p_{ce}/kPa	Relative Error/%
2	37.85	28.65	47.89	1106.02	-
3	28.03	21.36	35.26	818.42	26.37
4	26.17	20.07	33.02	766.44	6.62
5	25.50	19.61	32.24	748.05	2.56
6	25.19	19.40	31.88	739.49	1.24
7	25.01	19.29	31.68	734.81	0.69
8	24.91	19.22	31.56	731.99	0.42
9	24.84	19.18	31.48	730.15	0.28
10	24.79	19.15	31.43	728.89	0.19
11	24.76	19.12	31.39	727.99	0.14
12	24.73	19.11	31.36	727.32	0.10
13	24.72	19.10	31.34	726.81	0.08
14	24.70	19.09	31.33	726.41	0.06

The existing work of Soubra [43] investigated the bearing capacity problem by the same failure mechanism; however, the optimization is implemented separately about three independent components, that is $N_{\gamma e}$, N_{pe}, and $N_{c_f^* e}$, and the ultimate bearing capacity is obtained by the superposition method. Instead, an alternative that directly optimizes Equation (31) is also prevalent among many scholars. It turns out that the latter tends to estimate the solution on the conservative side. Consequently, in this work, the direct optimization of Equation (31) is implemented.

In the linear M-C failure criterion with $n = 14$, $B = 1$ m, $\zeta = 1$, $\varphi = 30^\circ$, $c = 15$ kPa, $p = 10$ kPa, and $\gamma = 18$ kN/m^3, Tables 2–5 list the results of the bearing capacity and the corresponding bearing capacity factors of Soubra [43] for comparison. The results of the present paper show a good consistency with those of Soubra [43]; the maximum difference is approximately 5% in the case of non-earthquake. However, the difference would be up to 30% in the presence of an earthquake, which states clearly that the discrepancy between direct optimization and the superposition method may be significantly amplified by the earthquake loads. The difference in the dimensionless coefficient $N_{\gamma e}$ is the maximum among the three components while the rest is not significant.

Table 2. Values of seismic bearing capacity p_{ce}/kPa.

k_h	$\varphi/^\circ$							
	15		20		25		30	
	This Paper	Soubra [43]	This Paper	Soubra [43]	This Paper	Soubra [43]	This Paper	Soubra [43]
0	176.34	168.4	268.60	254.83	429.00	405.24	726.41	684.02
0.1	140.90	134.79	210.81	200.59	330.20	312.86	546.95	516.61
0.2	108.75	102.64	160.22	151.77	246.73	233.66	400.75	378.93
0.3	81.43	64.80	118.43	110.14	179.79	169.02	287.17	270.8
0.4	59.83	51.40	86.27	67.50	129.98	117.92	206.30	189.09
0.5	45.80	39.80	65.63	52.30	98.57	70.20	156.32	128.45

Table 3. Values of seismic bearing capacity factor $N_{\gamma e}$.

k_h	$\varphi/^\circ$							
	15		20		25		30	
	This Paper	Soubra [43]	This Paper	Soubra [43]	This Paper	Soubra [43]	This Paper	Soubra [43]
0	2.80	2.10	5.77	4.67	11.80	10.06	24.70	21.88
0.1	1.54	1.01	3.46	2.61	7.37	6.04	15.75	13.59
0.2	0.66	0.26	1.78	1.13	4.14	3.14	9.28	7.67
0.3	0.14	-	0.71	0.26	2.02	1.28	4.97	3.80
0.4	-	-	0.21	-	0.97	0.28	2.87	1.51
0.5	-	-	-	-	0.47	-	1.78	0.35

Table 4. Values of seismic bearing capacity factor N_{pe}.

k_h	$\varphi/^\circ$							
	15		20		25		30	
	This Paper	Soubra [43]	This Paper	Soubra [43]	This Paper	Soubra [43]	This Paper	Soubra [43]
0	3.98	3.95	6.51	6.41	10.95	10.69	19.09	18.46
0.1	3.10	3.07	5.07	5.02	8.49	8.35	14.70	14.34
0.2	2.22	2.07	3.71	3.62	6.27	6.17	10.87	10.67
0.3	1.42	-	2.50	2.25	4.37	4.22	7.70	7.54
0.4	0.82	-	1.59	-	2.91	2.47	5.27	4.97
0.5	0.50	-	1.03	-	1.99	-	3.71	2.85

Table 5. Values of seismic bearing capacity factor $N_{c_t e}$.

k_h	$\varphi/^\circ$							
	15		20		25		30	
	This Paper	Soubra [43]	This Paper	Soubra [43]	This Paper	Soubra [43]	This Paper	Soubra [43]
0	11.13	11.00	15.15	14.87	21.33	20.78	31.33	30.25
0.1	9.61	9.50	12.90	12.69	17.89	17.50	25.83	25.09
0.2	8.07	7.96	10.72	10.54	14.67	14.37	20.85	20.32
0.3	6.60	6.48	8.71	8.53	11.80	11.53	16.54	16.12
0.4	5.22	5.14	6.85	6.75	9.21	9.07	12.78	12.58
0.5	4.22	3.98	5.54	5.23	7.45	7.02	10.32	9.68

4.2. Parametric Study

Parametric analysis is conducted in non-associative soils encompassing the seismic coefficients and the nonlinear parameters. For convenience, the minor factors that have no impact on the final result are set as constant in the whole text: $B = 1$ m, $\gamma = 18\ \mathrm{kN/m^3}$. The other basic inputs parameters are set as $k_h = k_v = 0.2$, $p = 15$ kPa, $\zeta = 0.8$, $m = 1.6$, $c_0 = 15$ kPa, and $\sigma_t = 15$ kPa. The normality of the plastic flow rule is one of the basic assumptions in the limit analysis, whereas the dilatancy angle of the soil is not necessarily equal to the internal friction angle for the natural geomaterials, which indicates that the plastic flow is not associative. Therefore, the illustrations in Figure 4 present the influence of the nonlinear coefficient on the seismic bearing capacity of foundations concerning different seismic coefficients under associative and non-associative soils, respectively. It appears that the bearing capacity of foundations under non-associative soils is significantly smaller than that under associative soils, which implies that the previous assumption of the normality of plastic flow tends to overestimate the upper-bound of the bearing capacity. In addition, the influence of the vertical seismic coefficient is so slight that can be neglected

in the analysis compared to that of the horizontal seismic coefficient. To further investigate the intrinsic influence of the non-associative characteristic of soils on the bearing capacity of the foundations, Figure 5 displays the variation in the bearing capacity with a dilatancy coefficient under the nonlinear failure criterion. It is observed that the bearing capacity of the foundations increases with the increase in the dilatancy coefficient. In Figure 6, the failure criterion changes into a linear M-C criterion, where the dilatancy angle ψ can be calculated based on Equation (7) with a known internal friction angle. The observed result shows that the foundation can bear more loads in the case of a greater dilatancy angle; notably, such an improvement becomes more pronounced for soils with a higher internal friction angle.

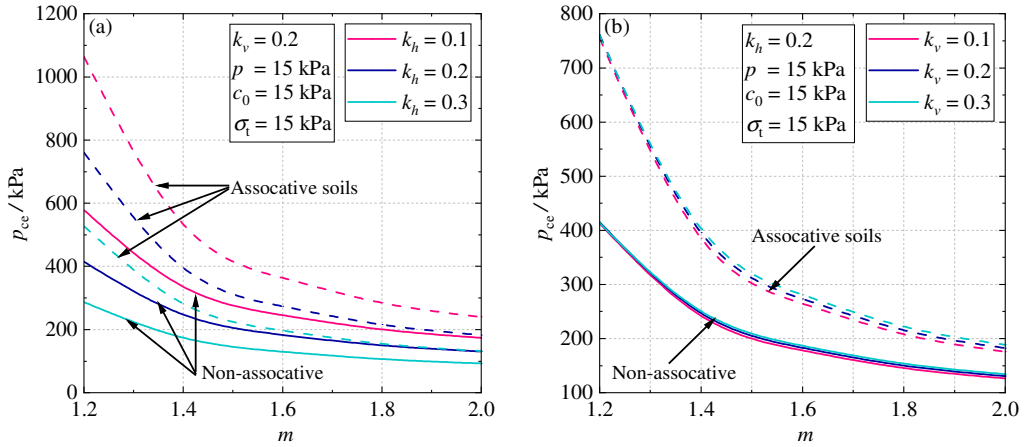

Figure 4. Seismic bearing capacity versus nonlinear coefficient and seismic coefficients: (**a**) horizontal seismic coefficient; (**b**) vertical seismic coefficient.

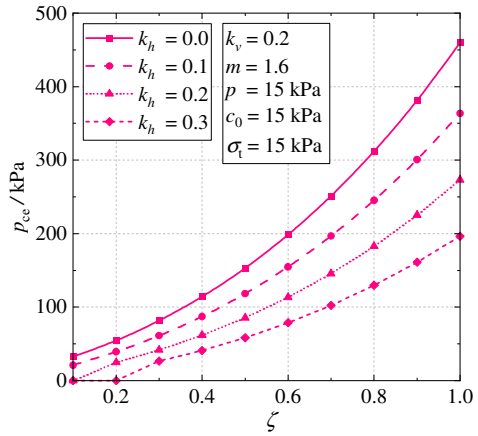

Figure 5. Influence of dilatancy coefficient on the seismic bearing capacity.

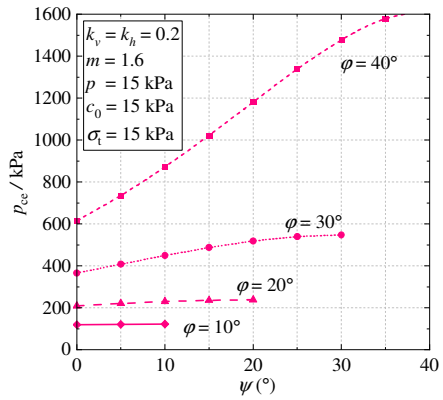

Figure 6. Values of seismic bearing capacity versus dilatancy angle and internal friction angle.

The consideration of earthquake loads is also necessary for the foundation located in an earthquake-prone area; therefore, earthquake analysis is also conducted in this work by the classic pseudo-static method. Not only are both the horizontal and vertical seismic coefficients considered, but also inertia forces acting on the soil mass, the lateral soil of footing, and the superstructure are included. The variation in the seismic bearing capacity with a vertical seismic coefficient is illustrated in Figure 7, where it is interestingly noted that when the horizontal seismic coefficient remains in a small range, such as no more than 0.2, the increase in the vertical seismic coefficient has a negative influence on the bearing capacity of the foundation, whereas a positive influence appears as the horizontal seismic coefficient becomes relatively greater. Such a strange phenomenon somewhat may be caused by the following reasons. First, this work assumes that the failure of the foundation is a process of footing sinking and lateral soil uplifting towards a certain direction. Assuming the vertical direction to be positive, in this case, the work rate done by the horizontal inertia force of the failure blocks is always positive while that of the vertical inertia force is not always positive because the failure blocks under the foundation produce negative work rates. The combined effect of horizontal and vertical seismic loads may result in a decreasing trend of the bearing capacity when the horizontal seismic coefficient is relatively small.

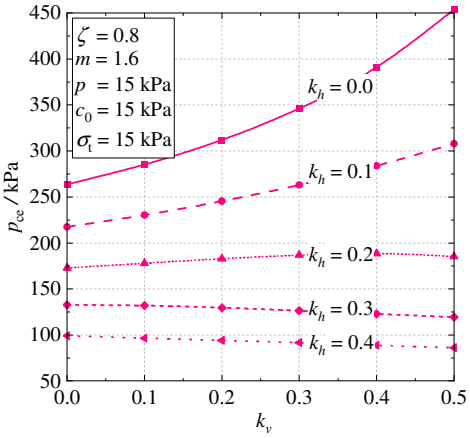

Figure 7. Influence of seismic coefficients on the seismic bearing capacity.

As illustrated in Figure 8, the equivalent surface surcharge has a favorable impact on the bearing capacity since it produces a negative work rate in the soil–foundation system and provides a resistance for preventing the foundation from failure. The improvement of the equivalent surcharge on the foundation is obvious in the absence of a horizontal seismic coefficient; then, the improvement effect gradually decreases with an increase in k_{h}. Figure 9 illustrates the influence of nonlinear parameters on the seismic bearing capacity of the foundations. The nonlinear coefficient m accounts for the curvature of the strength envelope, an increase in the nonlinear coefficient provokes a significant decrease in the bearing capacity, and the maximal reduction in the bearing capacity achieves 70.0% with a nonlinear coefficient ranging from 1.2 to 2.0 for $p = 25$ kPa. The same influence on the bearing capacity as the nonlinear coefficient is also observed from the uniaxial tensile strength, with a decrease of up to 82.4%. However, the initial cohesion has a beneficial effect on the bearing capacity of the foundation; an increase in the initial cohesion obtains a greater bearing capacity for the foundations. Notably, the variation in the bearing capacity with all nonlinear parameters behaves as a nonlinear tendency.

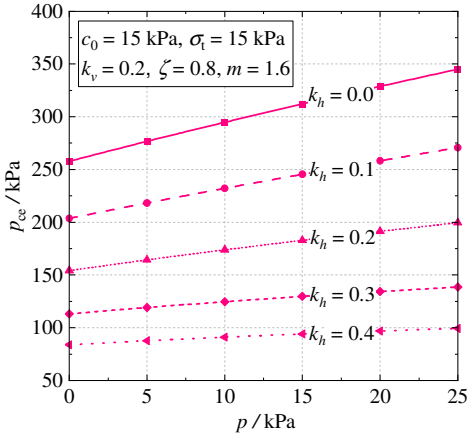

Figure 8. Seismic bearing capacity versus equivalent surcharge and horizontal seismic coefficient.

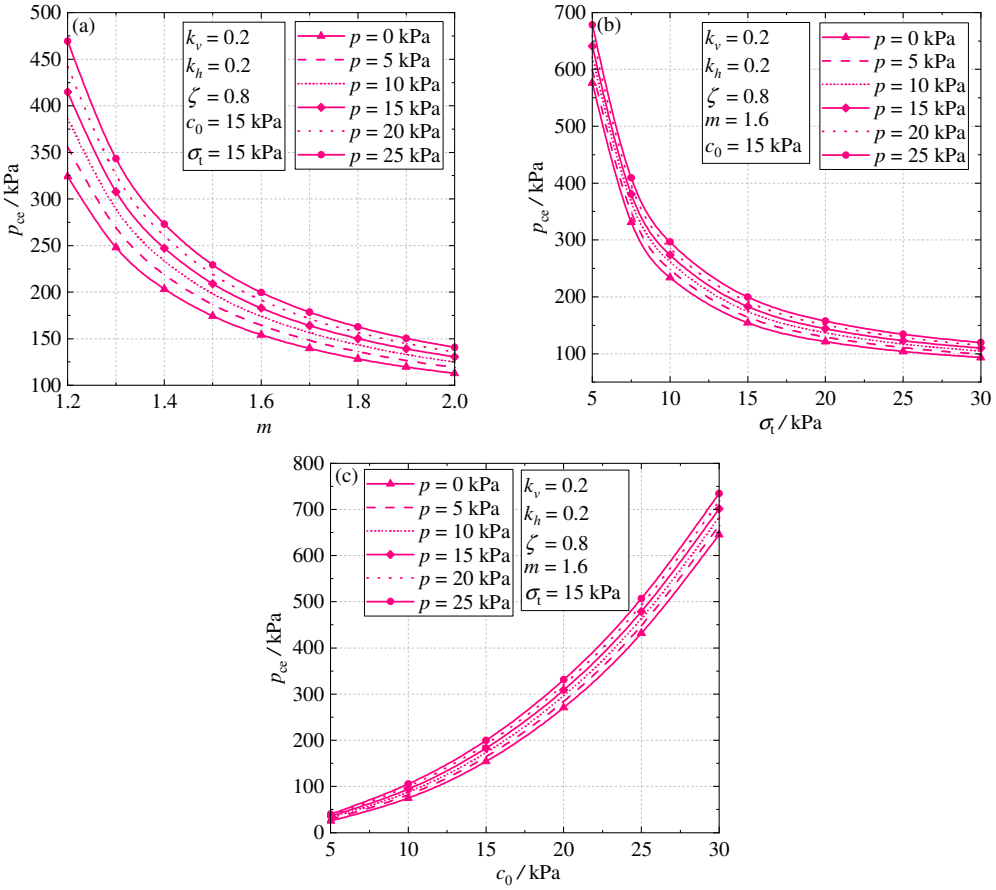

Figure 9. Influence of nonlinear parameters on the seismic bearing capacity: (**a**) initial cohesion; (**b**) uniaxial tension strength; (**c**) nonlinear coefficient.

4.3. Critical Failure Surface

This subsection discusses the effects of nonlinear parameters and seismic coefficients on the shape of critical slip surfaces, as presented in Figures 10 and 11. It is observed from Figure 10a that the surface surcharge has a small impact on the area of the critical slip surface. The increase in the initial cohesion leads to an extensive failure area and higher bearing capacity of the foundation; on the contrary, it is deserved to be noticed that the greater value of the nonlinear coefficient and uniaxial tensile strength results in a decrease in both failure regions and the bearing capacity, as shown in Figure 10c,d. As for the influence of seismic coefficients, Figure 11 displays the variation in the failure region of critical slip surfaces with horizontal and vertical seismic coefficients. It can be found that

the critical failure region becomes shallower as the horizontal seismic coefficient increases. However, the vertical acceleration intensity seems to not influence the failure region.

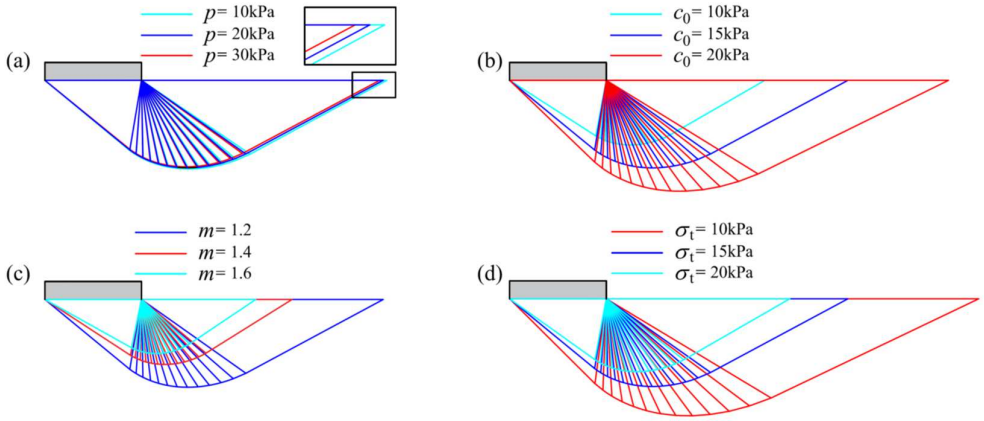

Figure 10. Critical failure surfaces for different p, c_0, m, and σ_t. (**a**) Effects of p. (**b**) Effects of c_0. (**c**) Effects of m. (**d**) Effects of σ_t.

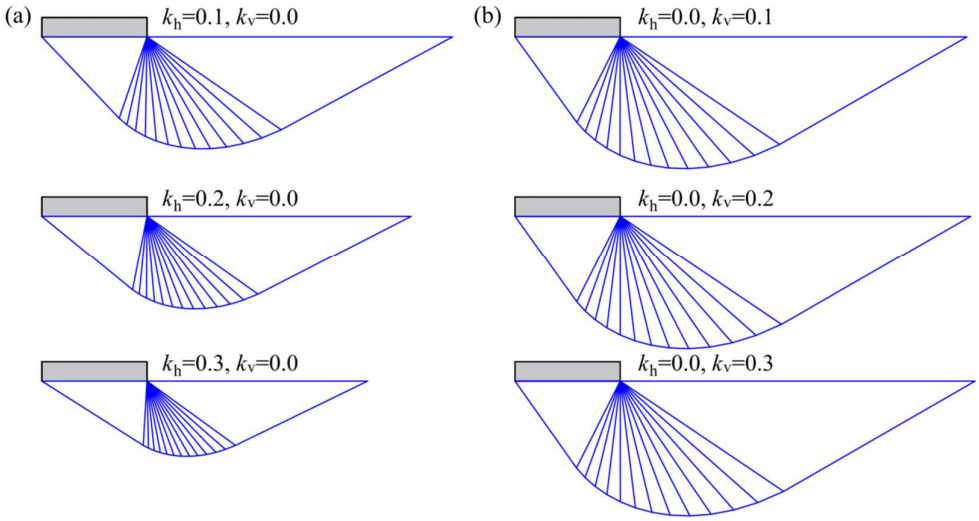

Figure 11. Critical failure surfaces with respect to different k_h and k_v. (**a**) Effects of horizontal force; (**b**) Effects of vertical force.

5. Conclusions

In terms of the upper-bound limit analysis, a non-symmetrical multi-block translational failure mechanism has been constructed for the investigation of the seismic bearing capacity of strip footings under the P-L strength criterion. The non-associative feature of soils is considered by introducing a dilatancy coefficient. Then, the new analytical solution is eventually derived from the energy equilibrium equation and is formulated as a multivariate optimization problem. The SQP algorithm is utilized herein to search for the least upper-bound solution. The proper number of rigid blocks of the failure mechanism is discussed based on the compromise between efficiency and accuracy. A comparison with the previous solutions is made in the linear condition to ensure the correctness of the present work, and the comparative result shows a good consistency with the literature. The detailed conclusions are summarized as follows:

In the process of searching the least upper-bound solution, two different optimization methods have a slight difference of approximately 5% in the absence of earthquakes; however, a significant difference of 30% might be attained for $k_h = 0.5$, which demonstrated that the presence of an earthquake would amplify the difference in different various optimization methods. In soils governed by the non-associative flow rule, the bearing capacity of the

foundations is significantly decreased with a decrease in the dilatancy coefficient. Especially in the linear condition, namely $m = 1$, the larger the internal friction angle is, the more obvious the influence of the non-associative feature on the bearing capacity is.

The uniaxial tension strength and nonlinear coefficient impose an adverse influence on the ultimate bearing capacity of the foundations, whereas the influence of an initial cohesion on the bearing capacity is favorable. In addition, the equivalent surface surcharge, as a positive factor, keeps the foundation from breaking by providing lateral soil pressure as the resistance. The k_{h} is always harmful to the bearing capacity, while the vertical seismic coefficient almost does not influence the bearing capacity of the foundations; interestingly, an increase in the vertical seismic coefficient may obtain a beneficial result to the foundation when the horizontal seismic coefficient is no more than 0.2. As expected, the horizontal seismic coefficient and surface surcharge have almost no influence on the shape of the critical failure mechanism; in contrast, the nonlinear parameters and horizontal seismic coefficient affect the critical failure region significantly, which demonstrated that the failure of the foundations tends to happen close to the surface with a small region when the adverse factors are significantly aggravated.

Author Contributions: Conceptualization, methodology, software, validation, formal analysis, investigation, resources, data curation, writing—original draft preparation, writing—review and editing, H.L.; visualization, supervision, project administration, funding acquisition, D.Z. All authors have read and agreed to the published version of the manuscript.

Funding: This research received no external funding.

Institutional Review Board Statement: Not applicable.

Informed Consent Statement: Not applicable.

Data Availability Statement: The data that support the findings of this study are available from the corresponding author upon reasonable request.

Conflicts of Interest: The authors declare that they have no conflicts of interest in this work.

Nomenclature

a_i = velocity discontinuity of the ith block
B = footing width
b_i = velocity discontinuity of the ith block
c_0 = initial cohesion
c_{t}, φ_t = equivalent shear strength
c^*, φ^* = shear strength for non-associative materials
c_t^*, φ_t^* = equivalent shear strength for non-associative materials
D = buried depth of footing
D_{int} = work rate of internal energy
F_i = external body loads
g = gravity acceleration
g_i = dimensionless expressions
k_{h}, k_{v} = seismic coefficients
m = nonlinear coefficient
n = number of blocks
$N_{c_{\mathrm{t}}^*\mathrm{e}}$, $N_{p\mathrm{e}}$, $N_{\gamma\mathrm{e}}$ = bearing capacity factors
P_{e} = load from the superstructure
p = equivalent pressure of lateral soils
p_{ce} = normalized bearing capacity
S = area of failure surface
T_i = external surface loads
V = volume of failure body
v_i = velocity of the ith block
$v_{i,i+1}$ = relative velocity between the ith block and the $i + 1$st block
W_{e} = work rate achieved by earthquake loads
W_{ext} = total external work rate
$W_{P_{\mathrm{e}}}$ = work rate produced by P_{e}
W_p = work rate achieved by lateral soils
W_γ = work rate achieved by soil weight
δ_i = angular variables of mechanism
$\dot{\varepsilon}_{ij}$ = plastic strain rate
γ = unit weight of soils
κ_i = angular variables of mechanism
$\dot{\lambda}$ = non-negative coefficient
θ_i = angle between v_i and vertical direction
σ_{ij} = effective stress
σ_{n} = normal stress at the failure surface
σ_{t} = uniaxial tensile strength
τ = shear stress at failure surface
τ_{t} = equivalent shear stress
Ψ = dilatancy angle
ζ = dilatancy coefficient

Appendix A

$$v_{i+1} = v_1 \cdot \prod_{k=1}^{i} \frac{\sin(\delta_i + \kappa_i - 2\varphi_t^*)}{\sin(\kappa_{i+1} - 2\varphi_t^*)},\ (i = 1, 2, 3 \cdots n) \tag{A1}$$

$$v_{i,i+1} = v_1 \cdot \frac{\sin(\delta_i + \kappa_i - \kappa_{i+1})}{\sin(\kappa_{i+1} - 2\varphi_t^*)} \prod_{k=1}^{i} \frac{\sin(\delta_i + \kappa_i - 2\varphi_t^*)}{\sin(\kappa_{i+1} - 2\varphi_t^*)} \tag{A2}$$

$$a_i = B \cdot \frac{\sin\delta_i}{\sin(\delta_i + \kappa_i)} \prod_{k=2}^{i} \frac{\sin\kappa_k}{\sin(\delta_k + \kappa_k)} \tag{A3}$$

$$b_i = B \cdot \frac{\sin\kappa_1}{\sin(\delta_1 + \kappa_1)} \prod_{k=2}^{i} \frac{\sin\kappa_k}{\sin(\delta_k + \kappa_k)} \tag{A4}$$

$$\begin{aligned} g_1 = \frac{\sin^2\kappa_1}{\sin^2(\delta_1+\kappa_1)} \sum_{i=2}^{n} \left[\frac{\sin\delta_i \sin\kappa_i}{\sin(\delta_i+\kappa_i)} \prod_{k=2}^{i-1} \frac{\sin^2\kappa_k}{\sin^2(\delta_k+\kappa_k)} \cdot \prod_{k=1}^{i-1} \frac{\sin(\delta_k+\kappa_k-2\varphi_t^*)}{\sin(\kappa_{k+1}-2\varphi_t^*)} \sin\theta_i \right] \\ + \frac{\sin\kappa_1}{\sin(\delta_1+\kappa_1)} \sin\delta_1 \sin\theta_1 \end{aligned} \tag{A5}$$

$$\begin{aligned} g_2 = \frac{\sin^2\kappa_1}{\sin^2(\delta_1+\kappa_1)} \sum_{i=2}^{n} \left[\frac{\sin\delta_i \sin\kappa_i}{\sin(\delta_i+\kappa_i)} \prod_{k=2}^{i-1} \frac{\sin^2\kappa_k}{\sin^2(\delta_k+\kappa_k)} \cdot \prod_{k=1}^{i-1} \frac{\sin(\delta_k+\kappa_k-2\varphi_t^*)}{\sin(\kappa_{k+1}-2\varphi_t^*)} \cos\theta_i \right] \\ + \frac{\sin\kappa_1}{\sin(\delta_1+\kappa_1)} \sin\delta_1 \cos\theta_1 \end{aligned} \tag{A6}$$

$$g_3 = \frac{\sin\delta_i}{\sin(\delta_i + \kappa_i)} \prod_{k=2}^{i} \frac{\sin\kappa_k}{\sin(\delta_k + \kappa_k)} \cdot \prod_{k=1}^{i-1} \frac{\sin(\delta_i + \kappa_i - 2\varphi_t^*)}{\sin(\kappa_{i+1} - 2\varphi_t^*)} \cdot \cos\left(\kappa_n - \varphi_t^* - \sum_{k=1}^{n} \delta_k\right) \tag{A7}$$

$$g_4 = \frac{\sin\delta_i}{\sin(\delta_i + \kappa_i)} \prod_{k=2}^{i} \frac{\sin\kappa_k}{\sin(\delta_k + \kappa_k)} \cdot \prod_{k=1}^{i-1} \frac{\sin(\delta_i + \kappa_i - 2\varphi_t^*)}{\sin(\kappa_{i+1} - 2\varphi_t^*)} \cdot \sin\left(\kappa_n - \varphi_t^* - \sum_{k=1}^{n} \delta_k\right) \tag{A8}$$

$$\begin{aligned} g_5 = \cos\varphi_t^* \sum_{i=1}^{n} \frac{\sin\delta_i}{\sin(\delta_i+\kappa_i)} \cdot \prod_{k=2}^{i} \frac{\sin\kappa_k}{\sin(\delta_k+\kappa_k)} \cdot \prod_{k=1}^{i-1} \frac{\sin(\delta_i+\kappa_i-2\varphi_t^*)}{\sin(\kappa_{i+1}-2\varphi_t^*)} \\ + \cos\varphi_t^* \sum_{i=1}^{n-1} \frac{\sin\kappa_1}{\sin(\delta_1+\kappa_1)} \frac{\sin(\alpha_i+\kappa_i-\kappa_{i+1})}{\sin(\kappa_{i+1}-2\varphi_t^*)} \prod_{k=2}^{i} \frac{\sin\kappa_k}{\sin(\delta_k+\kappa_k)} \prod_{k=1}^{i} \frac{\sin(\delta_i+\kappa_i-2\varphi_t^*)}{\sin(\kappa_{i+1}-2\varphi_t^*)} \end{aligned} \tag{A9}$$

References

1. Richards, R., Jr.; Elms, D.G.; Budhu, M. Seismic bearing capacity and settlements of foundations. *J. Geotech. Eng.* **1993**, *119*, 662–674. [CrossRef]
2. Dormieux, L.; Pecker, A. Seismic bearing capacity of foundation on cohesionless soil. *J. Geotech. Eng.* **1995**, *121*, 300–303. [CrossRef]
3. Silvestri, V.A. Limit equilibrium solution for bearing capacity of strip foundations on sand. *Can. Geotech. J.* **2003**, *40*, 351–361. [CrossRef]
4. Yang, X.L.; Yin, J.H. Upper bound solution for ultimate bearing capacity with a modified Hoek-Brown failure criterion. *Int. J. Rock Mech. Min. Sci.* **2005**, *42*, 550–560. [CrossRef]
5. Kumar, J.; Ghosh, P. Seismic bearing capacity for embedded footings on sloping ground. *Géotechnique* **2006**, *56*, 133–140. [CrossRef]
6. Nguyen, H.C.; Vo-Minh, T. Calculation of seismic bearing capacity of shallow strip foundations using the cell-based smoothed finite element method. *Acta. Geotech.* **2022**, *17*, 3567–3590. [CrossRef]
7. Zhong, J.H.; Li, Y.X.; Yang, X.L. Estimation of the seismic bearing capacity of shallow strip footings based on a pseudodynamic approach. *Int. J. Geomech.* **2022**, *22*, 04022143. [CrossRef]
8. Zhong, J.H.; Hou, C.T.; Yang, X.L. Bearing capacity of foundations resting on rock masses subjected to Rayleigh waves. *Soil Dyn. Earthq. Eng.* **2023**, *167*, 107791. [CrossRef]
9. Wang, N.; Xing, G.; Zhu, T.; Zhou, H.; Shi, Y. Propagating seismic waves in VTI attenuating media using fractional viscoelastic wave equation. *J. Geophys. Res. Solid Earth* **2022**, *127*, e2021JB023280. [CrossRef]
10. Huang, S.; Lyu, Y.; Sha, H.; Xiu, L. Seismic performance assessment of unsaturated soil slope in different groundwater levels. *Landslides* **2021**, *18*, 2813–2833. [CrossRef]

11. Wu, M.; Ba, Z.; Liang, J. A procedure for 3D simulation of seismic wave propagation considering source-path-site effects: Theory, verification and application. *Earthq. Eng. Struct. D* **2022**, *51*, 2925–2955. [CrossRef]
12. Zhai, S.Y.; Lyu, Y.F.; Cao, K.; Li, G.Q.; Wang, W.Y.; Chen, C. Seismic behavior of an innovative bolted connection with dual-slot hole for modular steel buildings. *Eng. Struct.* **2023**, *279*, 115619. [CrossRef]
13. Huang, S.; Huang, M.; Lyu, Y. Seismic performance analysis of a wind turbine with a monopile foundation affected by sea ice based on a simple numerical method. *Eng. Appl. Comp. Fluid.* **2021**, *15*, 1113–1133. [CrossRef]
14. Zhang, Z.L.; Yang, X.L. Pseudodynamic analysis of three-dimensional fissured slopes reinforced with piles. *Int. J. Geomech.* **2022**, *23*, 04022315. [CrossRef]
15. Li, J.; Cheng, F.; Lin, G.; Wu, C. Improved hybrid method for the generation of ground motions compatible with the multi-damping design spectra. *J. Earthq. Eng.* **2022**, *2022*, 2095059. [CrossRef]
16. Li, J.; Chen, M.; Li, Z. Improved soil–structure interaction model considering time-lag effect. *Comput. Geotech.* **2022**, *148*, 104835. [CrossRef]
17. Li, J.; Zhou, L.; Li, S.; Lin, G.; Ding, Z. Soil–structure interaction analysis of nuclear power plant considering three-dimensional surface topographic irregularities based on automatic octree mesh. *Eng. Struct.* **2023**, *275*, 115161. [CrossRef]
18. Keshavarz, A.; Nemati, M. Seismic bearing capacity analysis of reinforced soils by the method of stress characteristics. *IJST-T. Civ. Eng.* **2011**, *35*, 185–197. [CrossRef]
19. Keshavarz, A.; Fazeli, A.; Sadeghi, S. Seismic bearing capacity of strip footings on rock masses using the Hoek–Brown failure criterion. *J. Rock Mech. Geotech.* **2016**, *8*, 170–177. [CrossRef]
20. Casablanca, O.; Biondi, G.; Cascone, E.; Filippo, G.D. Static and seismic bearing capacity of shallow strip foundations on slopes. *Géotechnique* **2022**, *72*, 769–783. [CrossRef]
21. Ghosh, S.; Debnath, L. Seismic bearing capacity of shallow strip footing with coulomb failure mechanism using limit equilibrium method. *Geotech. Geol. Eng.* **2017**, *35*, 2647–2661. [CrossRef]
22. Izadi, A.; Mahsa, N.S.S.; Jamshidi Chenari, R.; Ghorbani, A. Pseudo-static bearing capacity of shallow foundations on heterogeneous marine deposits using limit equilibrium method. *Mar. Georesour. Geotec.* **2019**, *37*, 1163–1174. [CrossRef]
23. Nouzari, M.A.; Jamshidi Chenari, R.; Payan, M.; Pishgar, F. Pseudo-static seismic bearing capacity of shallow foundations in unsaturated soils employing limit equilibrium method. *Geotech. Geol. Eng.* **2021**, *39*, 943–956. [CrossRef]
24. Qin, C.B.; Chian, S.C. Kinematic analysis of seismic slope stability with a discretization technique and pseudo-dynamic approach: A new perspective. *Géotechnique* **2017**, *68*, 492–503. [CrossRef]
25. Yilmazoglu, M.U.; Ozocak, A. Bearing Capacity of Shallow Foundations on Unsaturated Silty Soils. *Appl. Sci.* **2023**, *13*, 1308. [CrossRef]
26. Li, Z.W.; Yang, X.L.; Li, T.Z. Static and seismic stability assessment of 3D slopes with cracks. *Eng. Geol.* **2020**, *265*, 105450. [CrossRef]
27. Sia, V.; Satyanaga, A.; Kim, Y. Effects of Heavy Rainfall on Shallow Foundations in Bukit Timah Granite in Singapore. *Appl. Sci.* **2022**, *12*, 9516. [CrossRef]
28. Zhang, Z.L.; Zhu, J.Q.; Yang, X.L. Three-dimensional active earth pressures for unsaturated backfills with cracks considering steady seepage. *Int. J. Geomech.* **2023**, *23*, 04022270. [CrossRef]
29. Chen, W.; Liu, Q.; Wang, E. The Effect of the Water Table on the Bearing Capacity of a Shallow Foundation. *Appl. Sci.* **2022**, *12*, 6571. [CrossRef]
30. Bralović, N.; Despotović, I.; Kukaras, D. Experimental Analysis of the Behaviour of Piled Raft Foundations in Loose Sand. *Appl. Sci.* **2023**, *13*, 546. [CrossRef]
31. Yang, X.L.; Li, L.; Yin, J.H. Seismic and static stability analysis for rock slopes by a kinematical approach. *Géotechnique* **2004**, *54*, 543–549. [CrossRef]
32. Zhong, J.; Hou, C.; Yang, X. Three-dimensional face stability analysis of rock tunnels excavated in Hoek-Brown media with a novel multi-cone mechanism. *Comp. Geotech.* **2023**, *154*, 105158. [CrossRef]
33. Zhang, X.J.; Chen, W.F. Stability analysis of slopes with general nonlinear failure criterion. *Int. J. Numer. Anal. Meth. Geomech.* **1987**, *11*, 33–50. [CrossRef]
34. Drescher, A.; Detournay, E. Limit load in translational failure mechanisms for associative and non-associative materials. *Géotechnique* **1993**, *43*, 443–456. [CrossRef]
35. Yang, X.L.; Wang, J.M. Ground movement prediction for tunnels using simplified procedure. *Tunn. Undergr. Space Technol.* **2011**, *26*, 462–471. [CrossRef]
36. Yang, X.L.; Huang, F. Collapse mechanism of shallow tunnel based on nonlinear Hoek-Brown failure criterion. *Tunn. Undergr. Space Technol.* **2011**, *26*, 686–691. [CrossRef]
37. Li, Z.W.; Yang, X.L. Active earth pressure for soils with tension cracks under steady unsaturated flow conditions. *Can. Geotech. J.* **2018**, *55*, 1850–1859. [CrossRef]
38. Huang, H.; Li, M.; Yuan, Y.; Bai, H. Theoretical analysis on the lateral drift of precast concrete frame with replaceable artificial controllable plastic hinges. *J. Build. Eng.* **2022**, *62*, 105386. [CrossRef]
39. Zhang, C.; Kordestani, H.; Shadabfar, M. A combined review of vibration control strategies for high-speed trains and railway infrastructures: Challenges and solutions. *J. Low Freq. Noise Vib. Act. Control* **2023**, *42*, 272–291. [CrossRef]

40. Huang, Y.; Huang, J.; Zhang, W.; Liu, X. Experimental and numerical study of hooked-end steel fiber-reinforced concrete based on the meso-and macro-models. *Compos. Struct.* **2023**, *309*, 116750. [CrossRef]
41. Sun, R.; Fu, L.; Cheng, Q.; Chiang, K.W.; Chen, W. Resilient Pseudorange Error Prediction and Correction for GNSS Positioning in Urban Areas. *IEEE Internet Things J.* **2023**, in press. [CrossRef]
42. Hou, C.; Zhong, J.; Yang, X. Three-dimensional stability assessments of a non-circular tunnel face reinforced by bolts under seepage flow conditions. *Tunn. Undergr. Space Technol.* **2023**, *131*, 104831. [CrossRef]
43. Soubra, A.H. Upper-Bound Solutions for Bearing Capacity of Foundations. *J. Geotech. Geoenviron. Eng.* **1999**, *125*, 59–68. [CrossRef]
44. Chen, W.F. *Limit Analysis and Soil Plasticity*; Elsevier Science: Amsterdam, The Netherlands, 1975. [CrossRef]
45. Yang, X.L.; Yin, J.H. Slope stability analysis with nonlinear failure criterion. *J. Eng. Mech.* **2004**, *130*, 267–273. [CrossRef]
46. Mabrouki, A.; Benmeddour, D.; Frank, R.; Mellas, M. Numerical study of the bearing capacity for two interfering strip footings on sands. *Comput. Geotech.* **2010**, *37*, 431–439. [CrossRef]